A little bit of lithium does a lot for hydrogen

Eva Zurek[a,1], Roald Hoffmann[a,2], N. W. Ashcroft[b], Artem R. Oganov[c,d], and Andriy O. Lyakhov[c]

[a]Department of Chemistry and Chemical Biology, Baker Laboratory, and [b]Laboratory of Atomic and Solid State Physics and Cornell Center for Materials Research, Cornell University, Ithaca, NY 14853; [c]Department of Geosciences and New York Center for Computational Science, Stony Brook University, Stony Brook, NY 11794-2100; and [d]Geology Department, Moscow State University, Moscow 11992, Russia

Contributed by Roald Hoffmann, July 28, 2009 (sent for review June 29, 2009)

From detailed assessments of electronic structure, we find that a combination of significantly quantal elements, six of seven atoms being hydrogen, becomes a stable metal at a pressure approximately 1/4 of that required to metalize pure hydrogen itself. The system, LiH_6 (and other LiH_n), may well have extensions beyond the constituent lithium. These hypothetical materials demonstrate that nontraditional stoichiometries can considerably expand the view of chemical combination under moderate pressure.

high pressure | hydrogen metallization | lithium chemistry

Three lines of thought—call them obsessions—impelled this investigation: (*i*) thinking of new pathways to promote and enhance the metallization of hydrogen, (*ii*) more generally the potential stability of new compounds with unusual stoichiometries under high pressures, and (*iii*) proposals for the design of new superconductors. As will be seen, we find two surprising ways (making good chemical sense) for the first, as well as sound theoretical evidence for the second. Based upon what is already known about possible superconductivity in metallic hydrogen, we find indications for the third.

LiH, crystallizing in the NaCl structure with a band gap of 4.99 eV (1), is one stable point in the Li/H phase diagram, the only one other than the elements at ambient conditions. It remains stable at higher pressures; the reaction $Li + \frac{1}{2}H_2 \rightarrow LiH$ is computed to be exothermic at all of the pressures we have considered. Calculations predict that pressure-induced metallization and transformation to the CsCl structure occur simultaneously at approximately 329 GPa (2). The results of our density functional theory (DFT) calculations on LiH are given in the supporting information (SI).

Hydrogen also vehemently resists metallization. At 320 GPa, it becomes black, indicating considerable reduction of the band gap under compression (3). Yet, it does not become metallic at the highest static pressures reached so far—342 GPa (4). Experimental and theoretical work indicates that combination with tetravalent atoms, as in the group 14 hydrides (5–13), may significantly lower the metallization pressure of H_2. It has also previously been pointed out that a second component, seen as an impurity in one point of view, may potentially reduce the pressure required to metalize H_2 (14).

Our computational results on the LiH_n phases ($n > 1$) suggest two strategies to metalize hydrogen, both achieved by the admixture of an electropositive element: (*i*) through Li^+ stabilizing the formation of H^- entities in an environment of H_2 units, accompanied by pressure-induced overlap of the H^- ("impurity donor band") and the H_2 σ_u^* bands and (*ii*) electron transfer from Li to H_2 σ_u^* levels with consequent metallization. In Fig. 1*A*, we schematically show the standard pressure-induced band broadening, which will eventually lead to the metallization of hydrogen. In Fig. 1 *B* and *C*, our two proposals are sketched.

These approaches will be illustrated below in detail for LiH_2 and LiH_6, although we have explored a variety of stoichiometries (LiH_n, n = 2–8) over pressures ranging from 0 to 300 GPa. In all of these phases, extended hydrogen networks begin to emerge at pressures still below those computed for the metallization of pure H_2. Interestingly, between ≈100 and 165 GPa, all become stable or metastable. All are metallic.

LiH_2, Hydrides, and Hydrogen Molecules

Our DFT calculations indicate that the ground state enthalpy of formation of LiH_2 (relative to LiH and H_2) becomes negative at approximately 120 GPa (or 2.4-fold compression). The best structure we have found, *P*4/*mbm* (space group 127), contains four formula units per cell, and therefore 12 valence electrons. As illustrated in Fig. 2*B*, a unit cell (Li_4H_8) contains four "guest" hydrogens, all part of H_2 units (white). The H–H distance is 0.76 Å at 150 GPa, close to that of an H_2 molecule in the gas phase or in the solid. When the pressure is doubled further to 300 GPa, the H–H bond length decreases only slightly, by 0.02 Å. The shortest distance between hydrogens belonging to two different H_2 units is 1.20/1.06 Å (along the *c* axis) at 150/300 GPa, indicating that a 1D chain-like network of hydrogen is developing with increasing pressure.

The mauve hydrogens in LiH_2 in Fig. 2*B* are different. They are part of an LiH "host" sublattice and their nearest neighbors are Li atoms (1.50/1.38 Å), whereas the closest hydrogen neighbors are at least 1.68/1.56 Å at 150/300 GPa. We will therefore refer to these as lone or hydridic hydrogens. LiH_2 can be thought of as containing interpenetrating Li^+H^- and H_2 sublattices. Its structure is reminiscent of Bi-III, Sb-II, Ba-IV and Sb-V, however in the elemental phases, the guest component is incommensurate with the host (see ref. 15 and references therein). Rb-IV and K-III (15) and the *tI*19 phase of Na (16) also have similar structures, but the host is made up of 16 atoms instead of 8.

The two types of hydrogens, differing much in their bonding, determine the electronic structure of LiH_2. In Fig. 3*A* the density of states (DOS) of LiH_2 at 0 GPa is shown: The main contribution to the peak lowest in energy comes from the σ_g bonding orbitals of the H_2 units (extended Hückel, eH, calculations confirm the H–H bonding in this band), whereas the peak just below μ_0 (ranging from approximately −1 to −5.8 eV) is primarily due to the hydridic atoms. There is little Li character in the occupied bands. Indeed, the DOS of LiH_2 agrees well with that computed for the charged hydrogen sublattice (see *SI*) indicating that the Li–H bonding is primarily ionic. The conduction band can be identified (via eH) as being derived from the σ_u^* orbitals of the H_2 units, with increasing Li contributions at higher energy. Note the one-dimensional nature of the σ_g (H_2) DOS.

The general features of the electronic structure of LiH_2 (Fig. 3 *A* and *B*) are represented schematically in Fig. 1*B*. With increasing pressure, the gap between the H_2 σ_g and H^- levels closes. More importantly, the H^- and unfilled H_2 σ_u^* bands approach each other; our DFT calculations predict that *P*4/*mbm*

Author contributions: E.Z. and R.H. designed research; E.Z. and R.H. performed research; A.R.O. and A.O.L. contributed new reagents/analytic tools; E.Z., R.H., N.W.A., and A.R.O. analyzed data; and E.Z., R.H., and N.W.A. wrote the paper.

The authors declare no conflict of interest.

[1]Present address: Department of Chemisty, University at Buffalo, State University of New York, 872 Natural Sciences Complex, Buffalo, NY 14260-3000.

[2]To whom correspondence should be addressed. E-mail: rh34@cornell.edu.

This article contains supporting information online at www.pnas.org/cgi/content/full/0908262106/DCSupplemental.

www.pnas.org/cgi/doi/10.1073/pnas.0908262106

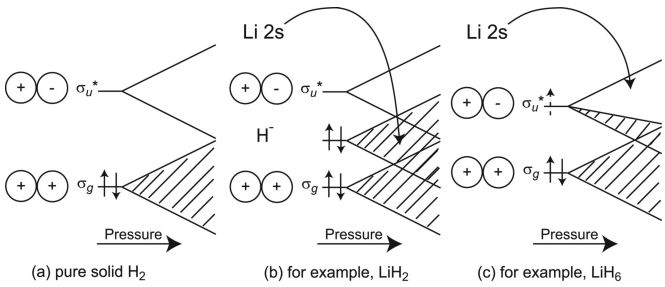

Fig. 1. Three conceptual ways to metallize hydrogen. (*A*) Standard view of metallization of H_2, arising from band broadening and eventual overlap. (*B*) Introduction of an ''impurity band'' of H^- between the σ_g and σ_u^* bands. (*C*) Partial filling of the σ_u^* band (the dotted arrow denotes occupancy by a fraction of an electron), lowers the pressure necessary for metallization.

LiH_2 becomes a semimetal at pressures slightly >50 GPa. By 120 GPa, the system also becomes more stable than $LiH + \frac{1}{2}H_2$. The band gaps obtained with DFT are typically too small, and H_2 itself is predicted to metalize at ≈240 GPa (17)—but it does not do so (3, 4). Given this discrepancy between theory and experiment, it is likely that our calculations also underestimate the pressure necessary to metalize LiH_2. Nonetheless, the metallization pressure we calculate is more than four times lower than the corresponding DFT values obtained for pure H_2.

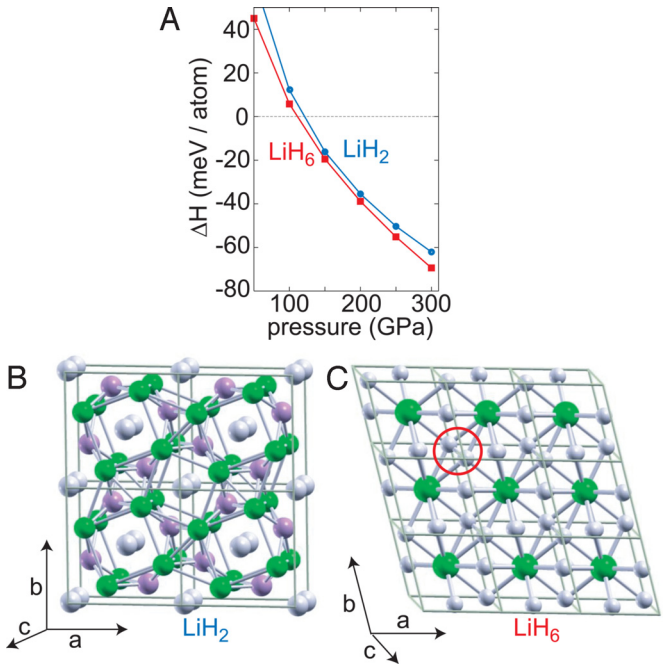

Fig. 2. Energetics and structure of LiH_2 and LiH_6. (*A*) Enthalpies of formation (meV/atom), of the most stable LiH_2 and LiH_6 structures as a function of pressure, and for temperature $T \to 0$. $\Delta H = H(LiH_n) - (n\text{-}1)/2\ H(H_2) - H(LiH)$, where the enthalpy of LiH is given for the rock salt structure, and the one for H_2 is given for the solid determined to be the most stable in ref. 17. Electronic and vibrational entropic contributions to the free-energy differences are not included, because it has been shown that for Li–Be alloys, they are approximately an order of magnitude smaller than ΔH (18). (*B* and *C*) Supercells of LiH_2 ($2 \times 2 \times 1$) (*B*) and LiH_6 ($3 \times 3 \times 1$) (*C*) at 150 GPa are also illustrated. Li atoms are shown as green, ''lone'' hydrogens are mauve, and hydrogens belonging to ''H_2'' units are white. A red circle indicates one of the dihydrogens in LiH_6. The structural parameters for LiH_2 and LiH_6 are given in the *SI* . Phonon calculations at 100/300 GPa did not reveal any imaginary frequencies, indicating that these are local minima. The zero-point energies have a negligible effect on the enthalpies of formation, being less than ≈7 meV per atom.

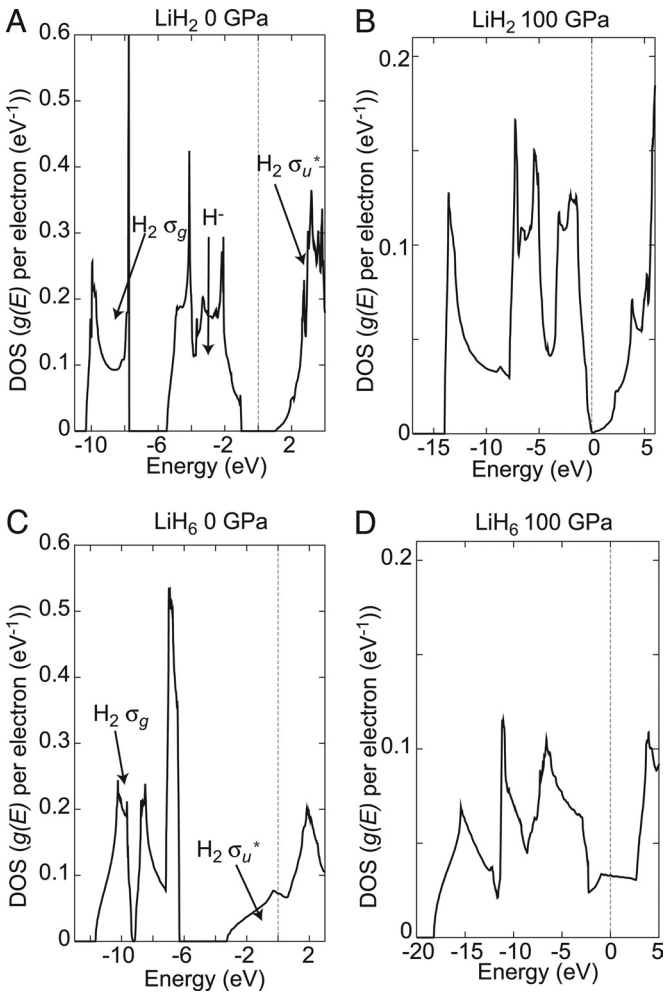

Fig. 3. DOS ($g(E)$/valence electron in eV^{-1}) of the most stable LiH_2 (*A* and *B*) and LiH_6 (*C* and *D*) structures at 0 GPa and 100 GPa. The dashed vertical lines are the zero temperature limit of the electron chemical potential, or the Fermi energy, E_F, for metallic states.

Fig. 3*B* reveals that at 100 GPa LiH_2 is just metallic, and the small density of states at the Fermi energy ($g(E_F)$/valence electron = 0.001 eV^{-1}) is reminiscent of the DOS calculated for compressed Li (19–21), rising only a little to 0.007 eV^{-1} at 300 GPa. For elemental Li, the 1s cores start to overlap with increasing pressure, and the valence electrons are pushed into the interstitial regions (19). Could it be that core overlap also occurs in LiH_2? Our calculations show that the width of the core Li 1s bands is 0.76 eV at 100 GPa and rises to 2.16 eV at 300 GPa, strongly indicative of core overlap. Indeed, the LiH_2 DOS is characterized by a pseudogap above a valence band maximum at every pressure studied (other than 1 atm). The closest distance between two Li atoms in LiH_2 is 2.06 and 1.65 Å at the aforementioned pressures. These distances are somewhat longer than in pure Li: 1.63 Å (*cI*16, 100 GPa), and 1.52 Å ($P4_132$, 300 GPa). It is very likely that in LiH_2 there are also Li–Li interactions that impel valence electrons into interstitial regions (calculations show that the maximum of the valence electron density for the Li sublattice is near the positions of the hydridic atoms in LiH_2, see Fig. S3 in *SI*). This remains to be explored further.

LiH_6, Metallic Because of Electron Transfer to H_2

By 110 GPa, LiH_6 is stable relative to LiH and H_2. For $P \geq 150$ GPa, it has the most negative enthalpy of formation of all of the

LiH_n structures we have found. The unit cell contains one formula unit ($R\bar{3}m$, space group 166) and therefore 7 valence electrons. Unlike LiH_2, in the optimized LiH_6 structure (Fig. 2*C*), no atoms are hydridic. All of the hydrogens belong to slightly stretched H_2 units. As will be seen, this is a consequence of electron transfer, and it is crucially important for the emerging electronic structure of the material. At 1 atm, the H–H bond length is computed to be 0.81 Å; this stretches slightly by 0.02 Å at a pressure of 50 GPa. Further compression up to 300 GPa has no effect on the shortest H–H distance. H_2 units with slightly stretched bonds have also been found in compressed germane (12). It should be mentioned that for LiH_6, as for the other LiH_n, we have strong indications that in the low-pressure regime ($P <$ ≈100 GPa), segregation and layering into slabs of LiH and H_2 is preferred.

The DOS of LiH_6 at 1 atm is given in Fig. 3*C*, (LiH_6 is not yet stable relative to LiH and H_2 at normal pressures) and it shows quite a surprise: The system is metallic. As in LiH_2, the lowest energy peak is traced to the σ_g bands. The Fermi level passes through a nearly free-electron-like region of the DOS, which we have identified (via eH) as being associated with the H_2 σ_u^* bands. Thus, LiH_6 can be viewed as composed of Li^+ and $(3H_2)^-$ fragments. The slightly stretched H–H bond is a result of the partial filling of the σ_u^* levels. In a molecular calculation, the bond in $(H_2)^q$ with a partial charge of $q = -1/3$ optimized to 0.80 Å, in good agreement with the H–H bond length in LiH_6 at 1 atm. Thus, metallicity—even at low pressure—occurs because of electron transfer as illustrated in Fig. 1*C*. And it is *not* (at low pressures) a result of the direct overlap of sublattice wave functions with compression, in stark contrast to LiH_2 and the recently studied group 14 hydrides (6–8, 10–12).

The electron-transfer-induced metallicity persists as LiH_6 becomes a stable phase. Also, as the pressure is increased, the gap between the σ_g and σ_u^* bands closes, as the DOS at 100 GPa in Fig. 3*D* reveals. Electron transfer from Li to H_2 σ_u^* continues to dominate. $g(E_F)$ is particularly high, 0.033 eV^{-1}/(valence electron), and remains nearly constant up to 300 GPa. Pressure has a nearly negligible effect on the intramolecular H–H distances. The intermolecular distances, on the other hand, decrease as expected.

The H_2 sublattice of LiH_6 is metallic at 100 GPa (see *SI*), whereas at the same pressure hydrogen is not. The sublattice is also ≈481 meV per proton less stable than the $P6_3/m$ H_2 structure. Why should this be? Consider Fig. 1*A*, a schematic sketch of metallization by band broadening and eventual overlap. If the H_2 bond is stretched, the energy of the molecular filled orbital will go up, and that of the empty one will go down (similar to Fig. 1*C*). As bands develop from the σ_g and σ_u^* levels under compression, they will merge at a lower pressure than for pure solid H_2.

Interestingly, at 1 atm, the volume of LiH_6 is a factor of two smaller than that of the optimized H_6 lattice, indicating that the ionic attraction between Li^+ and $3(H_2)^-$ results in "Madelung precompression." This is the primary reason for the ≈6 eV bandwidth of the σ_g in Fig. 3*C*. However, because of the presence of the Li^+ core, Madelung precompression is effective only in the low-pressure regime. For example, at 100 GPa, the volume of LiH_6 is ≈1.4 times greater than that of pure H_6.

Because of the high ratio of hydrogen in LiH_6, the distances between nearest-neighbor Li atoms are too large for core overlap to occur. The Li 1s bandwidth is 0.51 eV at 300 GPa (d(Li–Li) = 2.35 Å), approximately a factor of four less than for LiH_2 at the same pressure.

For LiH_6, the highest phonon frequencies of 2920/3590 cm^{-1} at 100/300 GPa (see *SI*) are reduced from the free H_2 vibron of 4,161 cm^{-1} (22). This is also a consequence of the population of the σ_u^*, and connected to the H_2 bond stretching, as observed in $SiH_4(H_2)_2$ (23). The aforementioned frequencies correspond to

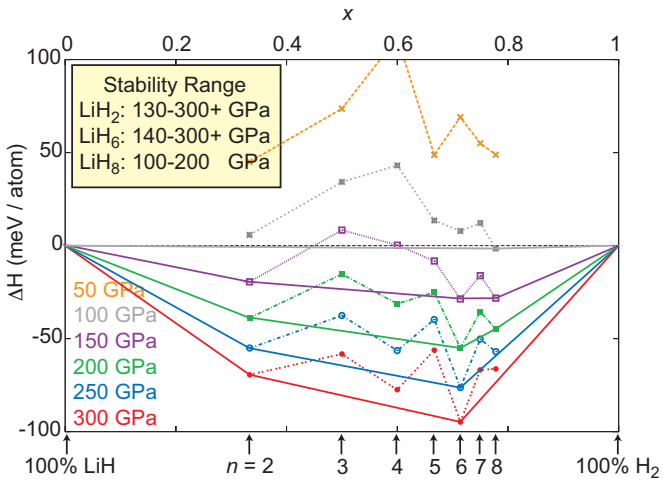

Fig. 4. Relative ground state enthalpies (with respect to LiH and H_2) of the most stable LiH_n (n = 2–8) solids. The abscissa x is the fraction of H_2 in the structures, and the black vertical arrows indicate the n in LiH_n. A tie line may be used to connect two phases, and if the enthalpy of a third falls below it, the first two will react to give the third. For example, a tie line between LiH_6 and LiH would show that a mixture of these could yield LiH_2 (but not LiH_3) at $P \geq$ 150 GPa, provided that the kinetic barriers are not too high. Lines are drawn connecting the stable phases at the different pressures considered, and their stability range is given in the *Inset*. Note that the estimated stability fields were determined with static enthalpies and may shift somewhat upon inclusion of dynamical effects (the zero-point motion of the nuclei). It is likely that LiH_2 and LiH_6 are also stable at $P >$ 300 GPa.

estimated Debye temperatures of 4,200/5,165 K. The substantial $g(E_F)$, and the large Debye temperatures for LiH_6 suggest that the electron–phonon coupling will be large. Moreover, the bands are wide, so that screening will reduce electron–electron repulsion (which works against pairing). Thus, LiH_6 may be another hydrogen-rich, high-temperature superconductor at experimentally accessible pressures.

Other Stoichiometries

We also studied LiH_n with n = 3–5, 7, and 8. Each has its own interesting peculiarities, but the essential underlying features have already been shown for the n = 2 and 6 cases above. LiH_3 is similar to LiH_2, with H_2 units and hydridic atoms. LiH_4 and LiH_8 are akin to LiH_6: They contain H_2 units with slightly stretched H–H bonds. In our calculations, LiH_5 shows two structures of nearly equal enthalpies (in the pressure range within which they are stable): one similar to LiH_2, and the other to LiH_6. Finally, LiH_7 also has two structures, one with H_2 units and the other with a complex hydrogenic network.

What we see in the various LiH_n structures is that some of the H_2 molecules are split up. Here is a way to think about it: Suppose Li transferred its valence electron to a single H_2, creating a fleeting negatively charged $(H_2)^q$, populating σ_u^* of H_2, weakening the H–H bond. For what q could the poor H_2 maintain bonding, albeit weakened? Molecular calculations supply an answer: $q = -1.2$ (for which H–H is stretched to 1.07 Å). If q is more negative, $(H_2)^q$ is not bound. This model suggests that $Li_{1.2}H_2$ is the limit; in a binary phase with more Li, any H_2 molecules are unlikely to exist.

The enthalpic trends of all of the LiH_n phases studied are shown in Fig. 4, a tie-line representation (18). The essential features of this diagram are the following: (*i*) of course, there is no stabilization for $n = 1$ and $n = \infty$ in LiH_n; (*ii*) stabilization begins to occur at ≈100 GPa for some n; by 200 GPa, all of the phases are stable or metastable relative to LiH and H_2; (*iii*) LiH_6 is the most stable phase for $P \geq$ 150 GPa; at 100 GPa, LiH_8 is

slightly more stable. There are regions of metastability for LiH_2 and LiH_8, and for a given pressure, various structures are within dynamical enthalpies of each other.

The optimum composition of Li_xH_y must have $y > x$, given the great donor strength of the electropositive Li, the incentive to stretch—if not break—the H–H bond by populating the σ_u^* band of the H_2, as well as the Madelung stabilization of Li^+H^-. Why the balancing act is best for LiH_6 is not yet clear to us.

Conclusion

Indeed, a little bit of Li does a lot for H_2—under pressure. All of the high-hydride phases with unusual stoichiometries (LiH_n, $n = 2–8$) become enthalpically stable relative to LiH and H_2. There is remarkable structural variety in the stable LiH_n; some contain only H_2 units, some both H_2 and H^- (or a host LiH lattice with H_2 guests). Every phase of LiH_n ($n > 1$) is computed to become metallic and stable or metastable in the range of ≈100–165 GPa, a pressure much lower that that required to metalize pure H_2. These structures provide ways to think about metalizing hydrogen by electron transfer from an electropositive element. Indeed, two strategies emerge: (*i*) stabilization of H^-, and thereby the introduction of a band between the filled and empty H_2 bands or (*ii*) population of the σ_u^* orbital of H_2. The phenomenon may not be limited to Li, and we have preliminary indications of similar behavior in other alkali high-hydride systems.

As a concluding observation, it may be noted that for pressures in the vicinity of 400 GPa, pure hydrogen, i.e., LiH_∞, may metalize as a ground-state quantum liquid (24). This suggests that in an Li–H alloy system, and at a pressure expected to be considerably lower than 400 GPa (based on the findings above), the possibility of eutectic-like behavior may arise for sufficient addition of hydrogen, but with the melting point dropping to temperatures close to zero. These could remain at very low values in the approach to the pure hydrogen limit, again suggesting consequent quantum liquid behavior and with possible quantum orderings now reflecting the statistical properties of the constituents.

Computational Methodology

Geometry optimizations and electronic structure calculations were performed by using DFT as implemented in the Vienna ab-initio simulation package (VASP) (25). The Perdew-Burke-Enzerhof (PBE) exchange–correlation functional (26), an energy cutoff of 500 eV, and all-electron plane-wave basis sets within the projector augmented wave (PAW) method (27) have been used. The *k*-point grids were generated using the Monkhorst–Pack scheme, and the number of divisions along each reciprocal lattice vector was chosen so that the product of this number with the corresponding real lattice constant was ≈50 Å. Phonon calculations were carried out by using VASP combined with PHON (28) on supercells of 189 (LiH_6) and 324 (LiH_2) atoms. Symmetry identification of the structures was carried out by using ISOTROPY (http://stokes.byu.edu/isotropy.html). For a given pressure, the lowest-enthalpy structures were found by using the evolutionary algorithm USPEX, which has been successfully tested and applied to many other systems (29–31). It also correctly predicts the rock salt structure for LiH between 0 and 200 GPa. For LiH_2/LiH_6, we have considered unit cells containing up to 4 and 2 formula units, respectively. Calculations were carried out between 0 and 300 GPa, in 50-GPa intervals. For a given cell size and stoichiometry, the USPEX calculations found the same space group and unit cell over the whole pressure range within which LiH_n was stable. The molecular calculations on $(H_2)^q$ were performed by using ADF (www.scm.com), and the extended Hückel (eH) computations with YAeHMOP (http://overlap.chem.cornell.edu:8080/YAeHMOP.html).

ACKNOWLEDGMENTS. We are grateful to L. N. Hand and M. Eremets for insightful discussions. This work was supported, in part, by National Science Foundation (NSF) Grants CHE-0613306, DMR-0601461, and DMR-0907425, and in part, by the NSF through TeraGrid resources provided by the National Center for Supercomputing Applications.

1. van Setten MJ, Popa VA, de Wijs GA, Brocks G (2007) Electronic structure and optical properties of lightweight metal hydrides. *Phys Rev B* 75:035204.
2. Lebegue S, Alouani M, Arnaud B, Pickett WE (2003) Pressure-induced simultaneous metal-insulator and structural-phase transitions in LiH: A quasiparticle study. *Europhys Lett* 63:562–568.
3. Loubeyre P, Occelli F, LeToullec R (2002) Optical studies of solid hydrogen to 320 GPa and evidence for black hydrogen. *Nature* 416:613–617.
4. Narayana C, Luo H, Orloff J, Ruoff AL (1998) Solid hydrogen at 342 GPa: No evidence for an alkali metal. *Nature* 393:46–49.
5. Ashcroft NW (2004) Hydrogen dominant metallic alloys: High temperature superconductors? *Phys Rev Lett* 92:187002.
6. Feng J, et al. (2006) Structures and potential superconductivity in SiH_4 at high pressure: En route to ''metallic hydrogen''. *Phys Rev Lett* 96:017006.
7. Pickard CJ, Needs RJ (2006) High-pressure phases of silane. *Phys Rev Lett* 97:045504.
8. Yao Y, Tse JS, Ma Y, Tanaka K (2007) Superconductivity in high-pressure SiH_4. *Europhys Lett* 78:37003.
9. Chen XJ, et al. (2008) Pressure-induced metallization of silane. *Proc Natl Acad Sci USA* 105:20–23.
10. Kim DY, et al. (2008) Crystal structure of the pressure-induced metallic phase of SiH_4 from ab initio theory. *Proc Natl Acad Sci USA* 105:16454–16459.
11. Martinez-Canales M, et al. (2009) Novel structures and superconductivity of silane under pressure. *Phys Rev Lett* 102:087005.
12. Gao G, et al. (2008) Superconducting high pressure phase of germane. *Phys Rev Lett* 101:107002.
13. Eremets MI, Trojan IA, Medvedev SA, Tse JS, Yao Y (2008) Superconductivity in hydrogen dominant materials: Silane. *Science* 319:1506–1509.
14. Carlsson AE, Ashcroft NW (1983) Approaches for reducing the insulator–metal transition pressure in hydrogen. *Phys Rev Lett* 50:1305–1308.
15. McMahon MI, Nelmes RJ (2006) High-pressure structures and phase transformations in elemental metals. *Chem Soc Rev* 35:943–963.
16. Gregoryanz E, et al. (2008) Structural diversity of sodium. *Science* 320:1054–1057.
17. Pickard CJ, Needs RJ (2007) Structure of phase III of solid hydrogen. *Nat Phys* 3:473–476.
18. Feng J, Hennig RG, Ashcroft NW, Hoffmann R (2008) Emergent reduction of electronic state dimensionality in dense ordered Li–Be alloys. *Nature* 451:445–448.
19. Neaton JB, Ashcroft NW (1999) Pairing in dense lithium. *Nature* 400:141–144.
20. Pickard CJ, Needs RJ (2009) Dense low-coordination phases of lithium. *Phys Rev Lett* 102:146401.
21. Yao Y, Tse JS, Klug DD (2009) Structures of insulating phases of dense lithium. *Phys Rev Lett* 102:115503.
22. Stoicheff BP High resolution raman spectroscopy of gases. 9. Spectra of H_2, HD and D_2. *Can J Phys* 35:730, 1957.
23. Strobel TA, Somayazulu M, Hemley RJ (2009) Novel pressure-induced interactions in silane-hydrogen. *Phys Rev Lett* 103:065701.
24. Ashcroft NW (2005) Metallic superfluids. *J Low Temp Phys* 139:711–726.
25. Kresse G, Hafner J (1993) Ab initio molecular dynamics for liquid metals. *Phys Rev B* 47:558–561.
26. Perdew JP, Burke K, Ernzerhof M (1996) Generalized gradient approximation made simple. *Phys Rev Lett* 77:3865–3868.
27. Blöchl P (1994) Projector augmented-wave method. *Phys Rev B* 50:17953.
28. Alfè D, Price GD, Gillan MJ (2001) Thermodynamics of hexagonal-close-packed iron under earth's core conditions. *Phys Rev B* 64:045123.
29. Glass CW, Oganov AR, Hansen N (2006) USPEX—evolutionary crystal structure prediction. *Comp Phys Comm* 175:713–720.
30. Oganov AR, Glass CW (2006) Crystal structure prediction using ab initio evolutionary techniques: principles and applications. *J Chem Phys* 124:244704.
31. Oganov AR, Glass CW, Ono S (2006) High-pressure phases of $CaCO_3$: Crystal structure prediction and experiment. *Earth Planet Sci Lett* 241:95–103.